Limiting Factors in Smartphone-Based Cross-Sensor Microstructure Material Classification*

Johannes Schuiki[1][0000−0002−6197−2327], Christof Kauba[1][0000−0002−2716−1360], Heinz Hofbauer[1][0000−0003−2969−1848], and Andreas Uhl[1][0000−0002−5921−8755]

Department of Artificial Intelligence and Human Interaction, University of Salzburg, Salzburg, Austria{jschuiki,ckauba,hofbauer,uhl}@cs.sbg.ac.at

Abstract. Intrinsic, non-invasive product authentication is the preferred way of detecting counterfeit products as it does not generate additional costs during the production process. Previous works achieved promising results for smartphone-based product authentication. However, while promising, the methods fail when enrollment and authentication are performed on different devices (cross-device). This work investigates the underlying reasons for the limitations in the practical application of cross-device intrinsic surface structure-based product authentication. In particular by utilising micro-texture classification approaches applied on images of zircon oxide blocks (dental implants) captured using a commodity smartphone device. The main result is that the device-specific artefacts (image sensor as well as image processing-specific ones) are so strong that they obfuscate the material microstructure. To be more precise, the device's intrinsic signal makes device identification easier to perform than the material authentication.

Keywords: intrinsic product authentication · material classification · microstructure texture features · dental ceramic blocks · camera source classification

1 Introduction

The wide-spread use and availability of mobile smartphone devices with built-in high quality cameras opened new possibilities for mobile applications such as classification of paving materials in urban environments [10], wood type identification [25], or personal authentication using biometrics [7]. Another recent application employing non-modified commodity smartphone devices is to verify a product's origin or to assure that a product stems from a certain manufacturer [26,3,8,24], denoted as product authentication. Counterfeit products do not only

* This research was partially funded by the Salzburg State Government within the Science and Innovation Strategy Salzburg 2025 (WISS 2025) under the project AIIV-Salzburg (Artificial Intelligence in Industrial Vision), project no 20102-F2100737-FPR.

cause economic damage to the original manufacturers especially counterfeit medical and health related products can directly harm the patients' health. Hence, manufacturers strive to implement ways to reliably detect non-genuine products, with several available commercial solutions for extrinsic, e.g. AuthenticVision, QLIKTag using NFC Tags as well as intrinsic mobile product authentication e.g. AlpVision, Bosch and Sepio's Logitrak.

Our previous work [22] addressed the practical applicability of using commodity off-the-shelf smartphone devices in combination with a clip-on macro lens to establish the authenticity of zircon oxide blocks, commonly used for dental ceramics in an intrinsic, non-intrusive way based on their surface's micro-texture. Material classification worked well in an intra-sensor ("one device") scenario, but the tested classifiers faced problems and limitations in the inter-sensor (cross-device) one. While a cross-device application is not an issue in many application settings (e.g. in biometrics) it is well-known to cause problems in other settings, e.g. in sensor forensics.

The main aim of this study is to investigate and understand the limiting factors for the cross-device intrinsic product authentication performance, their underlying reasons and in particular what happens during the image acquisition (i.e. the influence of the image signal processing tool-chain). This is an important step prior to developing appropriate countermeasures (i.e. training classifiers that work for smartphone devices unavailable during training) and can only be done in an explorative manner. Therefore, a second version of the zircon oxide block data set is acquired with more smartphone devices (7 in total), additionally capturing raw images as well. Furthermore, sensor identification experiments are performed as it turned out that sensor identification works better than the cross-device material classification. Sensor identification deals with establishing the origin of a digital image, i.e. linking an image to an image sensor/camera and can be done on two levels: manufacturer/type level or device/single instance level with the pixel response non-uniformity (PRNU) [14] being the most common approach for single instance sensor identification. There are other artefacts stemming from the image sensor, e.g. optical lens distortions, chromatic aberration, the layout of the physical pixel pattern on the sensor surface (Bayer pattern) as well as device-inherent processing steps from the image signal processor (ISP) which were successfully utilised as well [1,4]. The signal of these imaging artefacts might overlay the micro-structure texture features, impacting the cross-sensor material classification accuracy. This influence is evaluated utilising raw images, several variants of raw to RGB conversion and by applying an image denoising filter.

The rest of this work is organised as follows: Section 2 gives an overview on previous works about product authentication with a focus on smartphone-based mobile solutions. Section 3 introduces the dental ceramic data set, outlines the the micro-texture classification approaches and describes the experimental set-up. Section 4 lists and discusses the experimental results. Finally, Section 5 concludes this work and gives an outlook on future work.

2 Related Work

Product authentication can be categorised into intrinsic and extrinsic methods, where the latter ones rely on external properties added to the product. This can be as simple as a signed physical document, which can be easily forged, up to individual, hard-to-forge features that are embedded in each single product. These so called copy detection patterns (CDP) are usually a high resolution QR or 2D code printed with industrial printers on the product or its packaging. With the advancements in digital scanning technology and home printer equipment, CDPs are more often subject to successful illegal reproduction. Taran et al. [26,27] proposed a machine-learning framework (based on a one-class support vector machine) to explore the resistance of CDPs to illegal reproduction. They established a publicly available CDP dataset, tailored to real life conditions, named the "Indigo mobile dataset", captured using commodity smartphones (iPhone XS) under regular light conditions. Their reported results suggest that modern mobile phones allow to reliably authenticate CDPs under the considered classes of fakes. Cai et al. [3] proposed a deep learning product authentication approach for leather products based on texture features extracted from the material which are encoded into a non-detachable 2D barcode, which can be easily scanned and verified by consumers. Yan et al. [30] presented a framework that combines micro-texture features in combination with a QR code for anti-counterfeiting. Visual features and the QR code are registered on the assembly line and stored in a cloud and are then compared to images captured using a mobile phone for verification. The EU implemented the Falsified Medicines Directive (FMD) 2011/62/EU, based on product serialisation, i.e. a unique identifier in the form of a 2D barcode is added to each product, enabling to track and identify each medical package along the supply chain. It requires a central database and the packages to be equipped with safety features in order to avoid tampering.

Any form of external embedded features can be cumbersome to implement into a running production chain, require complex processing techniques, might add the demand for a back-end database infrastructure that needs to be administrated and increase the production costs. Thus, manufacturers prefer intrinsic methods, which are based solely on constant but discriminative intrinsic features of the product or its packaging material for product authentication. In practice, a further requirement is that the authentication can be done in a non-invasive way, i.e. without altering the product. The concept of surface micro-structures or so called physical non-cloneable functions (PUFs) is widely used in intrinsic product/material authentication, especially for paper based materials [11]. Paper PUFs use the fiber structure of paper as physical/intrinsic characteristic. In 2012, Voloshynovskiy et al. established the publicly available FAMOS data set [28], captured under different illumination conditions and with two different cameras and derived statistical authentication frameworks which achieved promising results. To overcome the main drawback of using micro-structures for product authentication - the large storage space required for the extracted feature information - the authors [2] suggested to use digital content fingerprints as a short and robust representation. In [9] the authors extended their previous work and

showed that it is feasible to uniquely identify packages based on micro-structure images acquired using an unmodified consumer smartphone without any special lighting or adaptation. They pointed out that the smartphone captured images suffer from non-linear distortions (lens distortions), geometrical distortions introduced by the user holding the phone in different manners and non-even, varying lighting conditions, all affecting the classification accuracy. However, no cross-device experiments between the smartphone and the handheld cameras have been performed. In a follow-up work [8] they utilised "SketchPrint", an approach previously introduced by the authors [29], which should provide reasonable invariance to varying lightning conditions and geometric distortions. They acquired a data set of 50 paper sheets with a commodity non-modified smartphone and achieved a reasonable performance. Schraml et al. [20,21] used micro-texture images of drug package material for product authentication in an open set scenario, which worked well in the intra-sensor scenario. Their later results in [21] showed that the classification capability is greatly reduced in a cross-sensor/device scenario with scaling issues (different dpi resolutions) as well as artefacts introduced during the image processing pipeline mentioned as reasons for the non-satisfactory performance. Sun et al. [24] utilised an efficient micro-structure orientation estimation technique, which models the entire propagation path of the light, to establish the authenticity of paper sheets using images captured with a mobile camera and its built-in flash. Sun et al. proposed the so called "LiquidHash" approach [23] for the detection of counterfeit liquid food products, based on the characteristics of air bubbles formed if the bottle is flipped. They utilised commodity off-the-shelf smartphone devices to capture a video stream of the bubble movement in combination with computer vision techniques to detect adulterated liquid products on a small data set (3 authentic and 8 counterfeit products).

While a sensor-aware classifier, specifically trained for each of the employed sensors could definitely improve the inter-sensor performance, the actual aim is to train a classifier that also works on smartphone devices not available during training. In practical applications the classification model is trained on a few particular devices, while the authentication should not be restricted to those devices but be possible on any modern off-the-shelf smartphone device so that even an end user can easily check if a product is genuine or counterfeit. The above works show that cross-device extrinsic product authentication as well as intrinsic micro-structure based material classification is feasible in practical applications using commodity smartphone devices. However, cross-device intrinsic micro-structure based product authentication has hardly been investigated. There is at least some evidence that the cross-device authentication performance is drastically reduced [21].

3 Experimental Setup

In the following, the database used within this study is explained in detail. Afterwards the employed texture classification tool-chain for the experiments Section 4 is described.

3.1 Database

Fig. 1: Unprocessed Zircon Oxide Ceramic Blocks.

The micro-texture database comprises of images acquired from the top side of zircon oxide blocks produced by three different manufacturers: 10 blocks produced by Ivoclar Vivadent, 6 by Dentsply and 16 by 3M. The different number of zircon oxide blocks is due to their limited availability. See Figure 1 for examples of such blocks. The acquisition setup is depicted in Figure 2. Four images, one on every top-side corner, were captured from every block using a macro lens *Agritix WIDK-24X01 Xylorix Wood Identification Tool* clipped onto the smartphone's camera with seven different smartphones (40, 24 and 64 samples per smartphone for *Ivoclar Vivadent*, *Dentsply Sirona* and *3M*, respectively). The distance between the block surface and the macro lens surface was 8 mm (This distance was best for successful auto-focusing). The macro lens has a circular illumination ring which was used on the brightest of the three settings during the acquisition to suppress the influence of varying lighting conditions and enhance the visibility of the surface micro-structure.

Checkerboard pattern images revealed that the fields of view between the various devices are similar but the resolutions are only coarsely matching. Therefore, a resolution normalization is applied by down-scaling the images to a fixed resolution of 2074x2765 using bilinear interpolation. Sensor resolutions and the scaling factors for each smartphone are listed in Table 1. Scaling the images with different factors naturally introduces resolution specific artefacts. Hence, one experiment in Section 4 deals with images without prior scale adjustments. The next step is to extract multiple patches by at first rotating the images to landscape orientation. Afterwards, the images are converted to gray-scale and nine patches of size 512×512 are cropped from the center as shown in

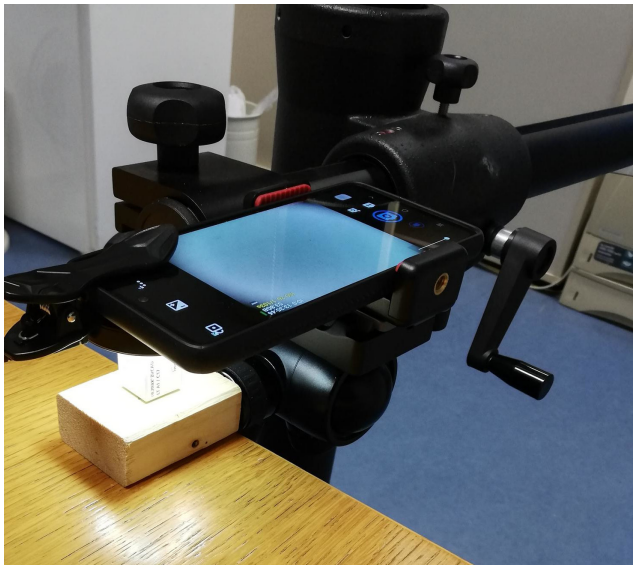

Fig. 2: Acquisition setup for the zircon oxide blocks, smartphone with clip-on macro lens.

Figure 3, resulting in 576, 216 and 360 patches for *Ivoclar Vivadent*, *Dentsply Sirona* and *3M*, respectively. This patching and down-scaling strategy avoids distortion (at the image boundaries) and black area (macro lens not perfectly aligned with the smartphone's lens) artefacts introduced by the macro lens. No further pre-processing (e.g. contrast enhancement) is employed to best preserve the micro-structures of the ceramic material and artefacts due to the sensor and ISP pipeline.

Table 1: Smartphones and their imaging sensor resolution.

Smartphone	Image Resolution	Scaling Factor
Google Pixel 4a (GP)	3024 x 4032	0.686
Huawei P20 Lite (H20)	3456 x 4608	0.600
Huawei P30 Pro (H30)	2736 x 3648	0.758
iPhone 11 (i11)	3024 x 4032	0.686
iPhone 13 Pro (i13)	3024 x 4032	0.686
Samsung Galaxy A52 (SG)	3468 x 4624	0.598
Xiaomi Mi A3 (XM)	3000 x 4000	0.691

Results from previous experiments [22] suggested that the smartphone inherent ISP greatly influences the cross-sensor performance. Hence, all images were

captured in raw in addition to the "normal" (ISP) image. Usually, the standard smartphone camera application does not allow to capture raw images. Hence, suitable camera applications were employed: OpenCamera for devices running Android and Halide Mark II for the iPhone devices. Two applications are used for conversion from the raw data, i.e. the Bayer pattern image, to an RGB image: Darktable (DT) and dcraw. Dcraw offers the possibility to set additional parameters such as *-a* (DCA) to average the whole image for white balance or *-d* to omit demosaicing, denoted as CFA (for color filter array) in the later experiments.

In order to remove PRNU and other sensor artefacts, images additionally underwent denoising by application of the BM3D [6] denoising filter. Results in Section 4 generated using denoised images are denoted with DN.

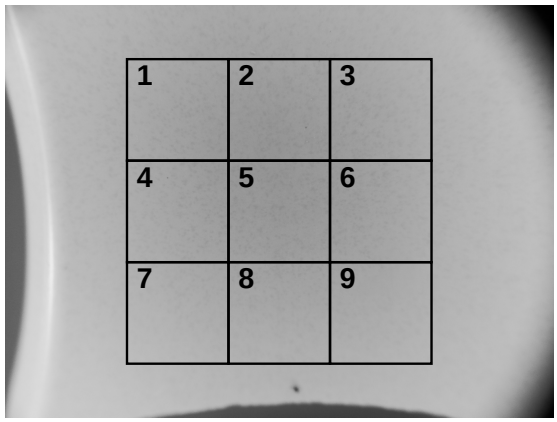

Fig. 3: Patch annotations in a zircon oxide block image.

3.2 Texture Classification Tool-Chain

Six distinct feature extraction techniques are employed in this study: Dense SIFT [13] (SIFT descriptors applied on a fixed-spaced grid), Dense Micro-block Difference (DMD) [15], Local Binary Pattern Histograms (LBP) [17], Local Phase Quantization (LPQ) [18] and Weber Pattern (WP) [16]. In addition to the aforementioned standard LBP variant, a second LBP feature descriptor is employed. LBP can be made rotational invariant by using a number of rotational shifts of the pattern equal to the number of points and taking the minimum. This method will be denoted as *ror* (n.b. this is not uniform LBP). Varying the radius of the LBPs can make it use differently sized structures and this will be denoted as

Rx where x is the radius in pixels. The extracted feature vectors (except the ones from the ror LBP) are subsequently encoded using improved Fisher vector encoding [19] in a similar way as originally proposed in [5]. They undergo a soft-quantization using a Gaussian mixture model and dimensionality reduction using principle component analysis. A support vector machine with linear kernel is utilized to classify the encoded features. For more details the interested reader is referred to our previous work [12].

The accuracy, defined as the number of correct classifications divided by the number of total classifications, is used as an evaluation metric to quantify the classification performance. The reported value in the experiments in Section 4 is the average accuracy, i.e. the arithmetic mean over all accuracies for a particular experiment.

4 Experimental Results

The experiments are divided into three parts: in (i) the acquired ceramic samples are classified with regard to their manufacturer in an intra-sensor scenario to verify that they contain enough texture information, in (ii) inter-sensor experiments are carried out, which constitutes a more realistic scenario, while in (iii) further experiments (camera classification) concerning the factors responsible for the bad results are done.

4.1 Intra-sensor ceramic texture classification

Table 2: Average ceramic classification accuracy in intra-sensor setup.

	ISP	ISP DN	DT	DT DN	DCA	DCA DN	CFA	CFA DN
SIFT	0.997	0.993	0.994	0.995	0.997	0.997	0.996	0.997
DMD	0.988	0.986	0.987	0.982	0.990	0.991	0.981	0.981
LBP	0.720	0.791	0.656	0.795	0.587	0.809	0.399	0.398
WP	0.760	0.770	0.752	0.787	0.760	0.804	0.670	0.675
LPQ	0.519	0.767	0.428	0.819	0.378	0.757	0.422	0.646

A random 50/50 training/evaluation data split, training using images from the same camera only, was performed. The average accuracy over all cameras for each imaging modality and feature is reported in Table 2. Obviously there is a signal strong enough for classification in all imaging modalities, e.g. SIFT reaches 99% classification accuracy for each modality.

Raw with denoising (DT DN, DCA DN, CFA DN) performs better than regular (ISP) images which include artefacts from the image processing pipeline. As the samples' patches in fig 4 show, the surface micro-structure texture components are hardly discernible. Thus, the imaging pipeline's artefacts clearly

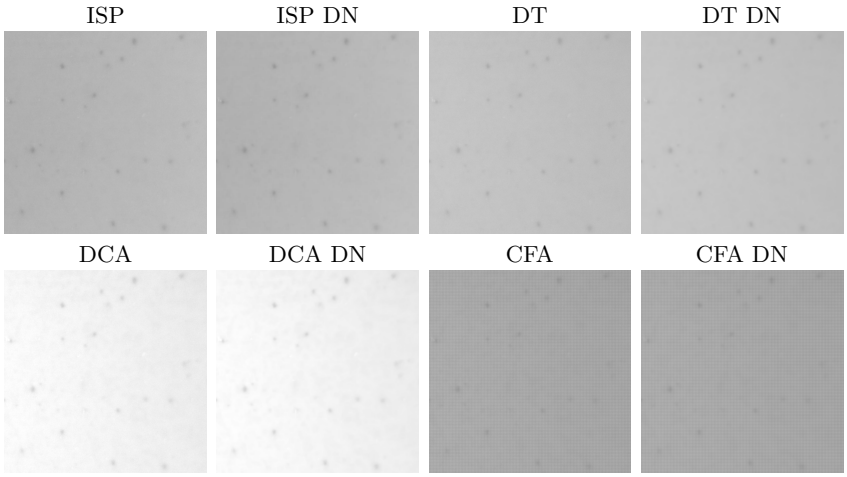

Fig. 4: Samples of ceramic images per imaging modality.

impact the ceramic sample image patches, lowering the classification accuracy and making raw the preferred choice.

4.2 Practical consideration: Inter-camera classification

Table 3: Average inter-sensor ceramic classification accuracy.

	ISP	ISP DN	DT	DT DN	DCA	DCA DN	CFA	CFA DN
SIFT	0.892	0.899	0.936	0.945	0.899	0.936	0.701	0.762
DMD	0.774	0.825	0.735	0.826	0.720	0.853	0.483	0.492
LBP	0.389	0.619	0.390	0.720	0.376	0.610	0.332	0.373
WP	0.484	0.676	0.595	0.698	0.593	0.638	0.362	0.366
LPQ	0.380	0.438	0.338	0.456	0.348	0.361	0.296	0.315
LBP R1	0.587	0.758	0.644	0.910	0.643	0.790	0.505	0.510
LBP R1 ror	0.567	0.769	0.966	0.911	0.672	0.776	0.500	0.517
LBP R4 ror	0.847	0.870	0.942	0.942	0.925	0.915	0.602	0.606

The results confirm that ceramic material classification is possible in the intra-device scenario while in practice it needs to be possible across different devices as well. To evaluate this cross-device scenario, a leave-one out training regime is used, i.e. train on 6 out of 7 ceramics and test on the 7th one, performed 7 times (for each ceramic). The (averaged) end results are given in Table 3.

The drop in classification accuracy compared to the intra-sensor scenario is quite substantial, especially for ISP. In most cases denoising improves the

classification results, with a best accuracy of 94%, but less than 70% in many other cases, which is not satisfactory. An interesting observation is that the drop in accuracy also happens with raw modes, in the best case using denoising there is a drop of 5%. Such a behaviour is not surprising for the ISP case, as each manufacturer and/or smartphone combination uses a different processing pipeline. Raw however, should not be influenced, with the resolution being the obvious difference (which is corrected, c.f. discussion in Section 3.1).

Table 4: Average ceramic classification accuracy in inter-sensor setup using SIFT features and DCA images.

		Test						
		GP	H20	H30	i11	i13	SG	XM
Train	GP	–	0.837	0.852	0.707	0.832	0.607	0.997
	H20	0.605	–	0.515	0.333	0.352	0.455	0.465
	H30	0.846	0.716	–	0.676	0.854	0.751	0.906
	i11	0.480	0.663	0.381	–	0.864	0.380	0.613
	i13	0.813	0.579	0.362	0.819	–	0.344	0.552
	SG	0.831	0.668	0.603	0.675	0.963	–	0.943
	XM	0.982	0.804	0.451	0.787	0.903	0.358	–

To validate if this behaviour is manufacturer or camera specific, an experiment where training is done on images from one camera and evaluated on images from another one, for all ISP/RAW/DN types and features, is conducted. The general trend is the same for all those combinations, so only SIFT on DCA is shown in Table 4 for reasons of brevity. Unfortunately our database is rather limited in terms of multiple smartphone models from the same manufacturer. However, for the Huawei smartphone cameras it is clearly a camera specific issue: if trained on Huawei H30, the H20 has the second worst performance of all cameras (highlighted in red colour in Table 4). On the other hand, the iPhones (i11 vs. i13 - highlighted in green in Table 4) work well in cross-training, still being inferior to many of the other tested combinations. Hence, in general it cannot be considered as a manufacturer specific effect but more a camera specific one. Also note that this is not reciprocal, i.e. if training on A performs well on B, training on B is not guaranteed to work well on A, e.g. for SG and XM (highlighted in orange in Table 4) - training on SG results in an accuracy of 94%, but training on XM only achieves 35% accuracy on SG.

4.3 Camera classification

The signal of the camera/ISP is strong enough to obfuscate the microstructure texture information used for material classification to a (sometimes strong) degree, raising the question if this can be used for camera classification. To test this, a leave-one material out cross-validation for camera classification

Table 5: Average sensor identification accuracy.

	ISP	ISP DN	DT	DT DN	DCA	DCA DN	CFA	CFA DN
SIFT	0.966	0.870	0.880	0.725	0.894	0.770	0.977	0.995
DMD	0.934	0.923	0.879	0.750	0.863	0.716	0.990	0.996
LBP	0.910	0.559	0.823	0.490	0.842	0.580	0.983	0.969
WP	0.796	0.497	0.393	0.375	0.443	0.480	0.962	0.947
LPQ	0.655	0.373	0.694	0.335	0.529	0.390	0.898	0.914
LBP R1	0.935	0.879	0.859	0.606	0.862	0.712	0.999	0.997
LBP R1 ror	0.981	0.880	0.527	0.563	0.883	0.690	0.999	0.996
LBP R4 ror	0.865	0.805	0.692	0.549	0.703	0.615	0.990	0.986

is performed. The results are given in Table 5. Camera classification works well with regular images processed by the ISP (98% accuracy) while raw ones perform worse in most cases. However, if the Bayer pattern is kept visible, the classification rate even reaches 99% accuracy. So apparently there are two signals able to identify the camera: the Bayer pattern and the image processing pipeline. What is more, the color filter arrays between models from the same manufacturer are different enough to differentiate between the devices.

Table 6: Classification accuracy results CFA unscaled.

	Texture Classification		Sensor Identification	
	CFA	CFA DN	CFA	CFA DN
SIFT	0.453	0.736	1.000	1.000
DMD	0.333	0.333	1.000	1.000
LBP	0.344	0.277	0.973	0.981
WP	0.539	0.755	0.666	0.399
LPQ	0.325	0.445	0.842	0.616

To rule out the influence of scaling (as a result of unifying the resolution), the camera identification experiment was carried out a second time using CFA samples without prior scaling. Figure 5 shows examples of unscaled CFA patches. The results are given in Table 6. While the texture classification performance is drastically reduced, sensor classification accuracy even reaches 100%, hereby allowing to deduce that scaling artefacts are not the reason for such a high accuracy.

4.4 Discussion of Results

For material classification the camera intrinsic signal has a detrimental effect on the classification as it obfuscates the material intrinsic one to a significant

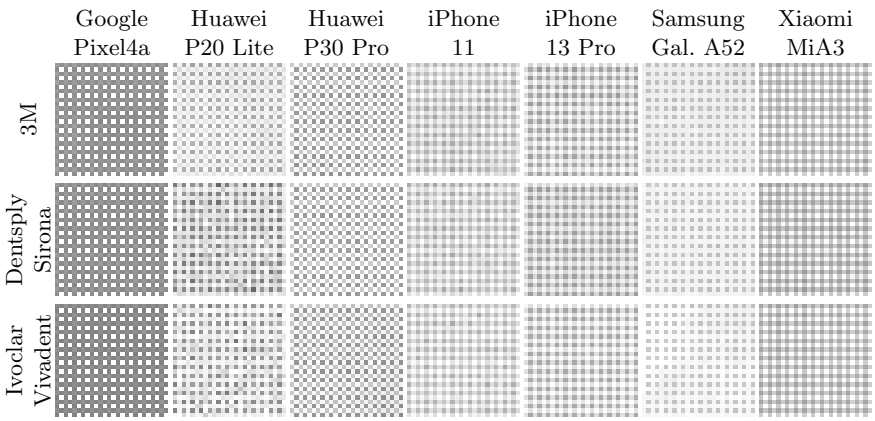

Fig. 5: Ceramic patches of size 26x26 converted with "dcraw -d". No down-scaling or denoising involved.

extent. This can partly be counteracted by capturing the images in raw format and denoising the images, as the camera specific signal is noise-like while the material specific signal is more coarse. This leads to a promising accuracy of 94% even in the cross-device scenario. However, it excludes a large number of devices, especially older ones not able to capture in raw mode. Hence, if they should be included, only the ISP images can be used, leading to a drop in accuracy to 87% (with denoising).
For device classification it became apparent that there are in reality two, probably not entirely independent, signals which can be used for camera identification. One is based on the sensor's intrinsics and image processing pipeline and the other one based on the Bayer-pattern and also the scaling done for resolution compensation. By using the second one (Bayer pattern), an incredibly high accuracy (99%) per patch can be achieved, but in practice it is still of little use as typical camera identification tasks are performed on regular images processed by the ISP rather than on raw ones, leaving us with the first one. Based on the first one (signal processing pipeline) the achievable accuracy is also high (98% per patch).

5 Conclusion

This work investigated the underlying reasons for the limitations in using unmodified off-the-shelf smartphone devices for intrinsic product authentication for ceramic materials based on their surface micro-structure. The experiments confirmed that there is an intrinsic signal from the material texture as well as one stemming from the camera itself which can be used to identify either one. The camera intrinsic signal, however, obfuscates the material intrinsic one to a significant extent, lowering the material classification accuracy, which can partly

be counteracted by capturing the images in raw mode. In reality there are two, probably not entirely independent, signals stemming from the imaging device which can be used for camera identification, one based on the sensor's intrinsics and image processing pipeline and the other one based on the Bayer-pattern. Even using the latter one an accuracy of 99% can be achieved.

Future work will include deep learning methods for classification and feature extraction. It is worth further investigating what constitutes the signal/ texture/ feature used for device identification. This is related to the topic of "cover source mismatch" in steganalysis. Hence, ideas from steganalysis to mitigate the cover source mismatch will be investigated too. With more precise information about the signal it can be removed to strengthen the material classification performance. Furthermore, we will acquire additional samples with different entities of the same smartphone model in order to identify the contribution of the ISP and the sensor specific artefacts.

References

1. Bayram, S., Sencar, H., Memon, N., Avcibas, I.: Source camera identification based on CFA interpolation. In: IEEE International Conference on Image Processing 2005. vol. 3, pp. III–69 (2005). https://doi.org/10.1109/ICIP.2005.1530330
2. Beekhof, F.P., Voloshynovskiy, S., Diephuis, M., Farhadzadeh, F.: Physical object authentication with correlated camera noise. In: Saake, G., Henrich, A., Lehner, W., Neumann, T., Köppen, V. (eds.) Datenbanksysteme für Business, Technologie und Web (BTW) 2013 - Workshopband. pp. 65–74. Gesellschaft für Informatik e.V., Bonn (2013)
3. Cai, S., Zhao, L., Chen, C.: Open-set product authentication based on deep texture verification. In: Peng, Y., Hu, S.M., Gabbouj, M., Zhou, K., Elad, M., Xu, K. (eds.) Image and Graphics. pp. 114–125. Springer International Publishing, Cham (2021)
4. Choi, K.S., Lam, E.Y., Wong, K.K.Y.: Automatic source camera identification using the intrinsic lens radial distortion. Opt. Express **14**(24), 11551–11565 (Nov 2006). https://doi.org/10.1364/OE.14.011551, https://opg.optica.org/oe/abstract.cfm?URI=oe-14-24-11551
5. Cimpoi, M., Maji, S., Kokkinos, I., Mohamed, S., Vedaldi, A.: Describing textures in the wild. In: 2014 IEEE Conference on Computer Vision and Pattern Recognition. pp. 3606–3613 (2014). https://doi.org/10.1109/CVPR.2014.461
6. Dabov, K., Foi, A., Katkovnik, V., Egiazarian, K.: Image denoising by sparse 3-d transform-domain collaborative filtering. IEEE Transactions on Image Processing **16**(8), 2080–2095 (2007). https://doi.org/10.1109/TIP.2007.901238
7. Das, A., Galdi, C., Han, H., Ramachandra, R., Dugelay, J.L., Dantcheva, A.: Recent advances in biometric technology for mobile devices. In: 2018 IEEE 9th International Conference on Biometrics Theory, Applications and Systems (BTAS). pp. 1–11 (2018). https://doi.org/10.1109/BTAS.2018.8698587
8. Diephuis, M., Voloshynovskiy, S., Holotyak, T.: Sketchprint: Physical object micro-structure identification using mobile phones. In: 2015 23rd European Signal Processing Conference (EUSIPCO). pp. 834–838 (2015). https://doi.org/10.1109/EUSIPCO.2015.7362500
9. Diephuis, M., Voloshynovskiy, S., Holotyak, T., Stendardo, N., Keel, B.: A framework for fast and secure packaging identification on mobile phones. In: Alattar,

A.M., Memon, N.D., Heitzenrater, C.D. (eds.) Media Watermarking, Security, and Forensics 2014. vol. 9028, p. 90280T. International Society for Optics and Photonics, SPIE (2014). https://doi.org/10.1117/12.2039638, https://doi.org/10.1117/12.2039638
10. Jain, S., Gruteser, M.: Recognizing textures with mobile cameras for pedestrian safety applications. IEEE Transactions on Mobile Computing **18**(8), 1911–1923 (2019). https://doi.org/10.1109/TMC.2018.2868659
11. JD, R.B., Cowburn, R., Jausovec, A., Petit, D., Seem, P., Xiong, G., Atkinson, D., Fenton, K., Allwood, D., Bryan, M.: Forgery:'fingerprinting'documents and packaging. Nature, Brief Communications **436**, 475 (2005)
12. Kauba, C., Debiasi, L., Schraml, R., Uhl, A.: Towards drug counterfeit detection using package paperboard classification. In: Advances in Multimedia Information Processing – Proceedings of the 17th Pacific-Rim Conference on Multimedia (PCM'16). Springer LNCS, vol. 9917, pp. 136–146. Xi'an, CHINA (2016). https://doi.org/10.1007/978-3-319-48896-7_14, http://dx.doi.org/10.1007/978-3-319-48896-7_14
13. Lowe, D.G.: Distinctive image features from scale-invariant keypoints. Int. J. Comput. Vision **60**(2), 91–110 (Nov 2004). https://doi.org/10.1023/B:VISI.0000029664.99615.94, http://dx.doi.org/10.1023/B:VISI.0000029664.99615.94
14. Lukas, J., Fridrich, J.J., Goljan, M.: Digital camera identification from sensor pattern noise. IEEE Transactions on Information Forensics and Security **1**(2), 205–214 (2006)
15. Mehta, R., Egiazarian, K.: Texture Classification Using Dense Micro-block Difference (DMD), pp. 643–658. Lecture Notes in Computer Science, Springer-Verlag, Berlin (2015). https://doi.org/10.1007/978-3-319-16808-1_43
16. Muhammad, G.: Multi-scale local texture descriptor for image forgery detection. In: Industrial Technology (ICIT), 2013 IEEE International Conference on. pp. 1146–1151 (2013)
17. Ojala, T., Pietikäinen, M., Mäenpää, T.: Multiresolution Gray-Scale and rotation invariant texture classification with local binary patterns. IEEE Transactions on Pattern Analysis and Machine Intelligence **24**(7), 971–987 (July 2002)
18. Ojansivu, V., Rahtu, E., Heikkila, J.: Rotation invariant local phase quantization for blur insensitive texture analysis. In: 2008 19th International Conf. on Pattern Recognition. pp. 1–4 (Dec 2008). https://doi.org/10.1109/ICPR.2008.4761377
19. Perronnin, F., Sánchez, J., Mensink, T.: Improving the Fisher kernel for large-scale image classification. In: Daniilidis, K., Maragos, P., Paragios, N. (eds.) Computer Vision – ECCV 2010. pp. 143–156. Springer Berlin Heidelberg, Berlin, Heidelberg (2010)
20. Schraml, R., Debiasi, L., Kauba, C., Uhl, A.: On the feasibility of classification-based product package authentication. In: IEEE Workshop on Information Forensics and Security (WIFS'17). p. 6. Rennes, FR (December 2017). https://doi.org/10.1109/WIFS.2017.8267659, https://doi.org/10.1109/WIFS.2017.8267659
21. Schraml, R., Debiasi, L., Uhl, A.: Real or fake: Mobile device drug packaging authentication. In: Proceedings of the 6th ACM Workshop on Information Hiding and Multimedia Security. p. 121–126. IH&MMSec '18, Association for Computing Machinery, New York, NY, USA (2018). https://doi.org/10.1145/3206004.3206016
22. Schuiki, J., Kauba, C., Hofbauer, H., Uhl, A.: Cross-sensor micro-texture material classification and smartphone acquisition do not go well together. In: Proc. of the

11th International Workshop on Biometrics and Forensics (IWBF'23). pp. 1–6. Barcelona, Spain (2023)
23. Sun, B., Tan, S.R.X., Ren, Z., Chan, M.C., Han, J.: On utilizing smartphone cameras to detect counterfeit liquid food products. In: Proceedings of the 20th Annual International Conference on Mobile Systems, Applications and Services. p. 551–552. MobiSys '22, Association for Computing Machinery, New York, NY, USA (2022). https://doi.org/10.1145/3498361.3538779, https://doi.org/10.1145/3498361.3538779
24. Sun, Y., Liao, X., Liu, J.: An efficient paper anti-counterfeiting method based on microstructure orientation estimation. In: ICASSP 2021 - 2021 IEEE International Conference on Acoustics, Speech and Signal Processing (ICASSP). pp. 2525–2529 (2021). https://doi.org/10.1109/ICASSP39728.2021.9415114
25. Tang, X.J., Tay, Y.H., Siam, N.A., Lim, S.C.: Mywood-id: Automated macroscopic wood identification system using smartphone and macro-lens. In: Proceedings of the 2018 International Conference on Computational Intelligence and Intelligent Systems. p. 37–43. CIIS 2018, Association for Computing Machinery, New York, NY, USA (2018). https://doi.org/10.1145/3293475.3293493, https://doi.org/10.1145/3293475.3293493
26. Taran, O., Tutt, J., Holotyak, T., Chaban, R., Bonev, S., Voloshynovskiy, S.: Mobile authentication of copy detection patterns: how critical is to know fakes? In: 2021 IEEE International Workshop on Information Forensics and Security (WIFS). pp. 1–6 (2021). https://doi.org/10.1109/WIFS53200.2021.9648398
27. Taran, O., Tutt, J., Holotyak, T., Chaban, R., Bonev, S., Voloshynovskiy, S.: Mobile authentication of copy detection patterns (2022). https://doi.org/10.48550/ARXIV.2203.02397, https://arxiv.org/abs/2203.02397
28. Voloshynovskiy, S., Diephuis, M., Beekhof, F., Koval, O., Keel, B.: Towards reproducible results in authentication based on physical non-cloneable functions: The forensic authentication microstructure optical set (famos). In: 2012 IEEE International Workshop on Information Forensics and Security (WIFS). pp. 43–48 (2012). https://doi.org/10.1109/WIFS.2012.6412623
29. Voloshynovskiy, S., Diephuis, M., Holotyak, T.: Mobile visual object identification: from sift-bof-ransac to sketchprint. In: Media Watermarking, Security, and Forensics 2015. vol. 9409, pp. 235–249. SPIE (2015)
30. Yan, Y., Zou, Z., Xie, H., Gao, Y., Zheng, L.: An IoT-based anti-counterfeiting system using visual features on QR code. IEEE Internet of Things Journal **8**(8), 6789–6799 (2021). https://doi.org/10.1109/JIOT.2020.3035697